Available online at www.sciencedirect.com
SCIENCE DIRECT®
Pergamon
Acta Materialia 51 (2003) 5399–5411
Acta MATERIALIA
www.actamat-journals.com

Yield surface of a simulated metallic glass

Alan C. Lund, Christopher A. Schuh *

Department of Materials Science and Engineering, Massachusetts Institute of Technology, 77 Massachusetts Avenue, Room 8-211, Cambridge, MA 02139, USA

Received 16 May 2003; received in revised form 12 July 2003; accepted 14 July 2003

Abstract

We perform molecular simulations of multiaxial deformation in a model metallic glass using a zero-Kelvin energy minimization technique. We find that there is a pronounced asymmetry between the magnitudes of the yield stresses in tension and compression, with the uniaxial compressive strength approximately 24% higher. By exploring a variety of biaxial stress states, we probe the plane-stress yield surface and find that it is not well-described by traditional yield criteria that depend only on the maximum shear stress. In contrast, the Mohr–Coulomb criterion, which includes an additional normal stress term, is found to describe the data quite well. Finally, the simulation results are shown to compare favorably with the available experimental data.

Keywords: Metallic glasses; Plastic deformation; Simulation; Mohr-Coulomb criterion

1. Introduction

Although metallic glasses exhibit extreme strength and many other desirable mechanical properties, their mechanisms of yielding and failure are still not thoroughly understood. At ambient temperature, metallic glasses deform by a process of *shear banding*, where plastic strain is highly localized into strips of nanometer-thickness and (often) macroscopic length. The operation of shear bands on the nanometer-scale gives rise to unique mechanical properties at macroscopic scales. For example, the very low values of tensile elongation recorded for amorphous metals are attributed to rapid failure along a single shear band [1–3]. In constrained modes of loading like compression or indentation, plastic yielding is observed, but it does not occur smoothly, instead exhibiting "load serrations" during brief intervals when the strain is carried by a single shear band [4–6]. These novel properties have been investigated in a variety of glassy alloys with very different compositions, and appear general to this class of materials.

One important consequence of shear localization in amorphous metals is that the macroscopic yield criterion may exhibit a dependence not only upon the maximum shear stress, but also upon the hydrostatic pressure or the normal stress acting on the shear plane. For example, whereas the classical von Mises or Tresca yield criteria predict a shear angle of $\theta = 45°$ to the axis of a uniaxial load,

* Corresponding author. Tel.: +1-617-452-2659; fax: +1-617-324-0053.
E-mail address: schuh@mit.edu (C.A. Schuh).

1359-6454/$30.00
doi:10.1016/S1359-6454(03)00396-3

several experimental studies on a variety of metallic glasses have found significantly different angles [1,2,7–11]. Examination of many independent experiments shows that they lie in the range $\theta \approx 39$–$45°$ in compression, and $\theta \approx 48$–$58°$ in tension. Many authors have noted that this asymmetry is symptomatic of a pressure- or normal-stress-dependent yield criterion.

Other works have directly examined the role of multiaxial stress states on the plastic yield of metallic glasses [7,9,12–16], and each of these studies has independently concluded that yield is not solely controled by the maximum shear stress. For example, early works by Donovan [7] and Ertürk and Argon [17] noted some asymmetry between the values of the yield stress for states of net tension and compression in Pd- and Co-based metallic glasses, respectively. More recently, Lowhaphandu, Lewandowski and co-workers [9,14,15] have used combined uniaxial-plus-pressure loading to explore the yield and failure of Zr-based metallic glasses. These authors showed a small pressure-dependence of the yield stress, again manifested as higher strengths in compressive loading states as compared with states of net tension. Flores and Dauskardt [13] have used notched tensile specimens to explore the regime of high tensile triaxiality. Finally, a recent study by Vaidyanathan et al. [16] used instrumented indentation coupled with finite-element analysis, to reveal a deviation from the von Mises criterion in a Zr-based amorphous alloy.

Although the experimental studies described above all suggest a failure of the classical von Mises or Tresca criteria for metallic glasses, they do not conclusively identify the form of the yield criterion, or provide a fundamental basis for this effect. With the exception of the analytical model of Flores and Dauskardt [13] for high tensile triaxialities, we know of no theoretical works that link the glassy structure with an asymmetric yield criterion. We expect that a fundamental explanation for the asymmetry can be found by considering the physical processes that underlie shear banding. Mechanistically, shear bands in metallic glasses are recognized as self-assembled structures of smaller units of plasticity, often called *shear transformation zones* (STZs), which comprise a local shear shuffle among a small cluster of ~10–50 atoms. Because the dominant physical mechanisms behind glass structure and deformation are generally localized to this very fine scale, atomistic modeling is a common method to elucidate the fundamental physics of glass formation, structure, and deformation. For example, many authors have investigated glass formation by quenching molten alloys or by mixing elemental metals in molecular simulations [18–24]; these simulations have reproduced most all the important features of glass formation and structure. Additionally, there are many computational studies of metallic glass deformation at both high and low temperatures [25–31]. These simulations have provided strong theoretical insight into the shear localization into bands at low temperature, as well as the dynamics of homogeneous flow at high temperature.

In this paper, we perform atomistic simulations of metallic glass deformation under multiaxial stress states, and explicitly map the yield surface in plane-stress space. These simulations support an atomic-scale origin for the asymmetric yield behavior of metallic glasses, in broad agreement with the experimental literature.

2. Simulation details

We perform molecular static simulations of deformation in metallic glasses, using a model binary alloy system composed of equal fractions of what are nominally Cu and Zr atoms. The simulations are performed in three-dimensional computational cells with periodic boundary conditions applied in all three principle directions, *x*, *y*, and *z*. The initial structure is built by growing randomly oriented FCC atom arrays from multiple seed locations in a Voronoi-type construction, with the species of each atom (Cu or Zr) chosen randomly to obtain an approximately equiatomic global composition. The as-built structure is allowed to relax to a local equilibrium using the method of conjugate gradients [32], with the atoms interacting via simple metallic interatomic potentials of the form [33,34]:

$$\phi(r_{ij}) = \frac{A}{r_{ij}^4} + \frac{B}{r_{ij}^8} + Cr_{ij} + D \tag{1}$$

with r_{ij} being the separation distance between two atoms i and j. The variables A, B, C, and D are constants specific to the type of atoms interacting; Table 1 lists these values for the Cu–Cu, Cu–Zr, and Zr–Zr interactions, chosen to fit the elastic constants of these elements in Refs. [33,34]. The nominal radii of the Cu and Zr atoms, based on the minima of the pair potentials, are ~2.7 and ~3.3 nm, respectively.

The global stress tensor of the structure is calculated based on the interatomic potentials using [35],

$$\sigma_{ab} = \frac{1}{2V}\sum_{\substack{i=1\\ j\neq i}}^{N}\sum_{j=1,}^{N}\frac{\partial\phi}{\partial r_{ij}}\cdot\frac{r_{ij}^{a}r_{ij}^{b}}{r_{ij}} \tag{2}$$

where V is the volume of the computational cell, N is the total number of atoms, and r_{ij}^{a} and r_{ij}^{b} are the separation distances between atoms i and j along any two given principle directions a and b, respectively. Upon relaxation, the random solid–solution structure spontaneously amorphizes, but generally has a non-zero stress state. To allow the initial glassy structure to find a local energy minimum with near-zero stress components, we repeatedly adjust the dimensions of the computational cell in small increments along the principle directions, and reposition each atom accordingly. By intelligently choosing the dimensional adjustments and allowing complete relaxation after each, the structure is guided toward a low-stress state (all stress components less than 10 MPa).

Two approximately equiatomic starting structures were obtained in the manner described above, containing 2609 or 2781 atoms. A radial distribution function (RDF) from the structure with 2781 atoms is shown in Fig. 1a, with a visual representation of the structure shown in Fig. 1b. The RDF for the 2609 atom structure was qualitatively (and nearly quantitatively) identical to that shown in Fig. 1a. All the data presented below have been obtained from the simulations starting from one of these two initial structures.

To explore the yield behavior of the amorphous structures, we deformed them by applying strain increments along the principle directions. The largest strain increment in any principle direction was set to 0.1%, in line with many previous simulations [27,34]. The remaining strain increments were judiciously chosen to generate a variety of plane-stress conditions ($\sigma_{zz}\approx 0$). While the strain increments along the x- and y-directions were held

Table 1
Constants used for the interatomic potentials (Eq. (1)), taken from Ref. [33,34]

	Cu–Cu	Cu–Zr	Zr–Zr
A (eV·Å^4)	30.7744	71.7076	149.3512
B (eV·Å^8)	744.52	2708.56	8313.28
C (eV·Å^{-1})	−0.03276	−0.04808	−0.07023
D (eV)	0.21095	0.339368	0.531656

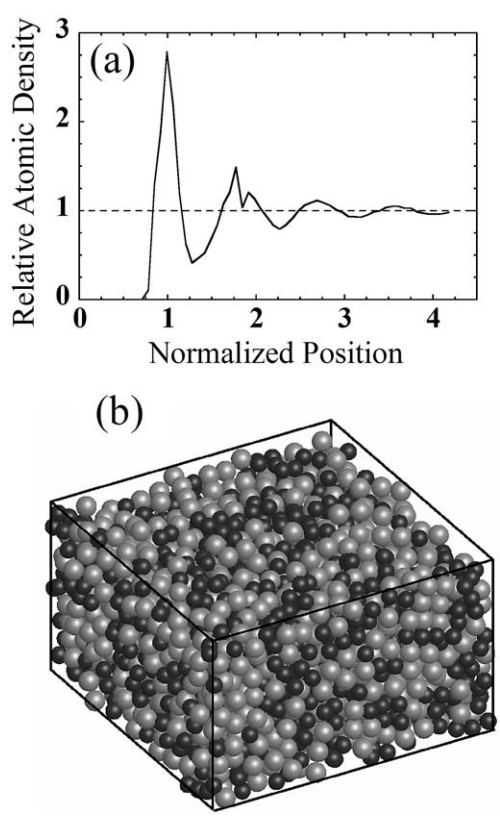

Fig. 1. (a) The radial distribution function and (b) a visual representation of one of the starting structures (2781 atoms), shown to demonstrate that the initial structures are fully amorphous. Lighter atoms represent Zr, while darker ones represent Cu. The frame surrounding the atoms in (b) is 4.5 × 4.5 × 2.6 nm.

constant, the increment along the *z*-direction was constantly adjusted to maintain a plane-stress state of loading. Following each strain increment the structure was again allowed to relax, and the stress state of the system was calculated using Eq. (2). The total strain state of the system is quantified using an equivalent strain ε_{eq} for a biaxial stress-state [36],

$$\varepsilon_{eq} = \frac{1}{1+\nu}\sqrt{\varepsilon_x^2 + \varepsilon_y^2 - \varepsilon_x\varepsilon_y + \frac{\nu}{(1-\nu)^2}(\varepsilon_x + \varepsilon_y)^2} \quad (3)$$

where ε_x and ε_y are the true strains along the x and y axes, respectively, and a constant value of $\nu = 0.36$ is used for purposes of calculation [33]. By repeating this straining process multiple times with different x and y strain increments, we have probed the full plane-stress yield surface.

3. Results

Stress–strain curves from an unbalanced biaxial compression test are shown in Fig. 2, and represent a typical example of the simulation output. The curves for both σ_{xx} and σ_{yy} show the same basic behavior: at low strains ($\varepsilon_{eq} \lesssim 2\%$), the deformation is reasonably linear and elastic, at high strains ($\varepsilon_{eq} \gtrsim 6\%$), the deformation is fully plastic, and between these extremes, there is a rather broad transition region. The exact limits of these regions are not well-defined; for analysis purposes, the curves are taken to be linear-elastic out to 2% equivalent strain. Using this standard, a least-squares fit of multiple uniaxial tension and compression curves provides a Young's modulus of $E = 65 \pm 5$ GPa, and we use this value for purposes of normalization in what follows. Also, we note that defining the linear-elastic region more strictly (i.e. up to maximum values of below 2%) gives values of the Young's modulus ranging up to approximately 80 GPa, which is more in line with the published experimental [37] and theoretical [34] results for Cu–Zr glasses.

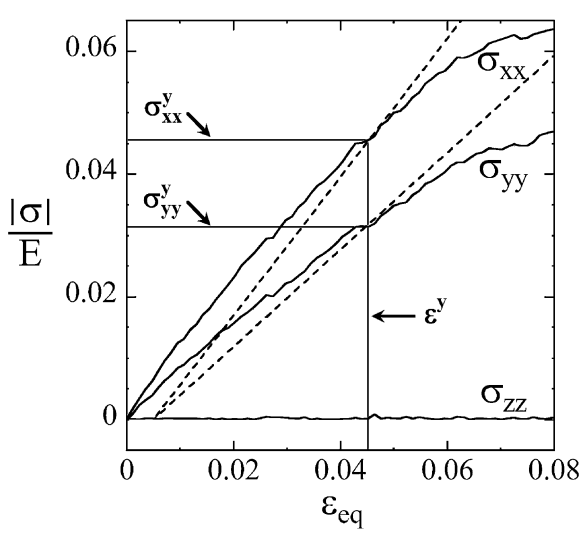

Fig. 2. A set of principle stress–strain curves from an unbalanced biaxial compression test. The offset method used to determine the stresses (σ^y_{yy} and σ^y_{xx}) and strain (ε^y) at yield is also demonstrated: the dashed lines are parallel to the linear-elastic regions of the σ_{yy} and σ_{xx} curves are offset by $\Delta\varepsilon = 0.5\%$, while the light lines show the yield stresses and strain determined from the intersection of the offset line with the σ_{xx} curve.

Fig. 2 also illustrates the standard offset method [36,38] used to determine the yield stress components σ^y_{xx} and σ^y_{yy}. A line is drawn parallel to the linear-elastic region of the dominant stress–strain curve (σ_{xx} in Fig. 2), and offset by a small amount $\Delta\varepsilon$. The intersection of the offset line with the curve gives the first yield stress component, i.e. σ^y_{xx}, as well as the equivalent strain at yield ε^y. The other yield stress component, i.e. σ^y_{yy}, is then identified as the value of σ_{yy} at ε^y. In all the cases, the second yield stress component determined in this manner is very close to that obtained by simply applying the same offset criterion to the second stress–strain curve, providing an internal consistency check for the method. This is illustrated in Fig. 2 with an offset of $\Delta\varepsilon = 0.5\%$; as discussed later, in some cases we have also used a more standard offset of $\Delta\varepsilon = 0.2\%$. The value of the uniaxial tensile strength determined in this manner (with $\Delta\varepsilon = 0.2\%$) is $\sigma^y_T = 1.8 \pm 0.2$ GPa, which agrees well with the experimental values in the range of 1.7–2.2 GPa for the yield of Zr-based glasses in pure tension [37,39]. Due to the enforcement of plane-stress conditions, the stress along the *z*-axis is negligible as shown in the example of Fig. 2.

In Fig. 3, we present the results of typical uniaxial tension and compression simulations performed on the same initial glass structure. These curves

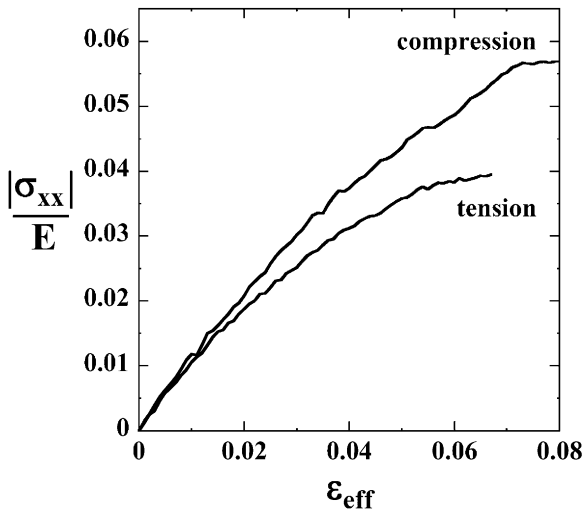

Fig. 3. The results of two uniaxial straining simulations using the same initial structure, one in compression and the other in tension, with only the curves from the non-zero stress axis shown. The simulated glasses are notably stronger in compression than in tension.

demonstrate an obvious asymmetry in the plastic mechanical response that we find to be a general characteristic of yield in our metallic glasses: the yield strength in compression is higher than the yield strength in tension. Based on the values from multiple such simulations, we find the yield stress in compression σ_C^y to be about 24% higher than that in tension σ_T^y.

The full plane-stress yield surface of our simulated glasses is shown in Fig. 4. Simulations were performed on both sides of the mirror-symmetry axis $\sigma_{xx} = \sigma_{yy}$, but since there is no structural anisotropy in the simulated metallic glasses, we have enforced this symmetry for all data points. In Fig. 4, we show two data sets, one obtained using the standard 0.2% offset common in experiments (Fig. 4a), and the other obtained using a larger 0.5% offset (Fig. 4b); the two resulting yield surfaces are quite similar. The primary qualitative difference between Figs. 4a and 4b is the greater relative scatter in the data obtained using the 0.2% offset, which results from a greater sensitivity to noise near the yield point in the stress–strain curve. The primary quantitative difference between these figures is the consistently lower magnitudes of the stress components obtained using the 0.2% offset,

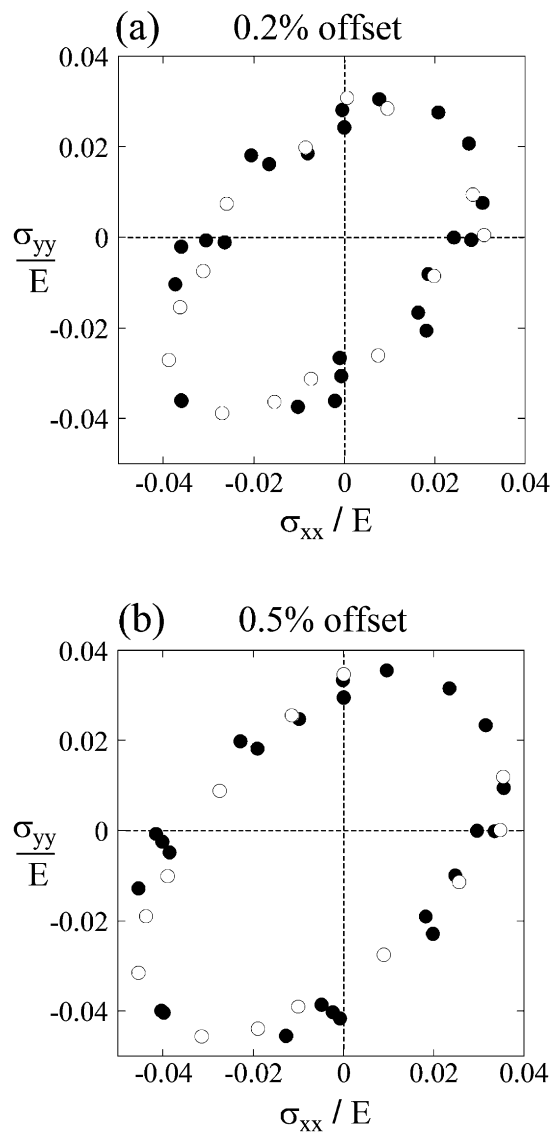

Fig. 4. The plane-stress yield surfaces ($\sigma_{zz} \approx 0$) obtained with (a) 0.2% offset and (b) 0.5% offset. The solid and open points represent the data from the 2609 atom and the 2781 atom initial structures, respectively. Both yield surfaces (a) and (b) show the same basic shape; the lobe in quadrant III is larger than that in quadrant I, reflecting the strength asymmetry between compression and tension noted in Fig. 3. Errors on each data point are ~0.002 in both principle directions.

as expected given the gradual nature of yielding observed in Fig. 2. Since the general shapes of the two yield surfaces are qualitatively identical, we use the 0.5% offset data in all our subsequent analysis and discussion, to take advantage of the reduced scatter. As indicated by the uniaxial tension and compression tests shown in Fig. 3, the yield surfaces shown in Fig. 4 are distinctly asymmetric, with the elastic envelope defined by the data in quadrant III being considerably larger than that in quadrant I. This asymmetry is in direct proportion to the strength differential observed in uniaxial loading.

Before proceeding to a more detailed discussion, we note that while the results presented above were obtained by the methods described in Section 2, we have also extensively validated these results by applying different potentials and boundary conditions not presented here. For example, in addition to the 3-D periodic simulation cell, we have also considered cells periodic in only two dimensions (equivalent to an infinite thin sheet). Simulations were also conducted using several different interatomic potentials. In all cases, we have seen the same qualitative results, and hence conclude that the behavior illustrated in Figs. 2–4 is characteristic of the metallic glass structure, and not a byproduct of the chosen boundary conditions or interatomic potentials.

4. Discussion

The asymmetric yield behavior observed in Figs. 3 and 4 is in general agreement with all the experiments described in Section 1, and suggests that the maximum shear stress alone cannot predict yield in metallic glasses. In the sections that follow, we first identify the atomic processes controling plasticity in our simulations, and then proceed to a discussion of the yield criterion on this atomistic basis. Finally, we compare our simulation results to existing experimental data.

4.1. Deformation mechanisms

Here, we briefly analyze the atomic positions during the biaxial compression test of Fig. 2, and identify those atoms which participate in plastic strain evolution during any given strain increment. Every time the simulated structures are strained, each atom is moved a prescribed distance based on the applied strain increment, and then allowed to relax to a local energy minimum. To identify which atoms are participating in any plastic deformation, we compare the final location of each atom to its expected location based solely on a forced elastic motion. This analysis reveals that after relaxation, the atoms are never located precisely where continuum elasticity would predict, but are nearly always within about 0.015 nm of this location. Atoms which move significantly more than this can be identified as those participating in a local configurational rearrangement, i.e. plastic deformation.

In Fig. 5a, we show the fraction of atoms that are instantaneously participating in a plastic rearrangement as a function of the equivalent strain. This analysis reveals that the number of participating atoms is small but non-zero at virtually all levels of strain. Close inspection also reveals that each significant spike in Fig. 5a coincides with an observable fluctuation in the stress–strain curve. For example, the largest of the spikes in Fig. 5a coincides very closely with the yield strain marked in Fig. 2. We also observe numerous “pre-yield” plastic events, which is consistent with the gradual transition from linear-elastic to fully plastic deformation noted above. Significant atomic rearrangements prior to large-scale yielding have also been observed by other researchers using molecular simulations [27,31]. Further, there is precedent in the experimental literature, where several investigators have observed discrete plastic strain events prior to the onset of full plasticity in uniaxial compression [1,40]. These observations underscore the fact that the “plastic yield point” is an ill-defined concept in the present context (and perhaps in metallic glasses in general), and must be regarded solely as a convenient engineering construct. In this paper, it is best to regard the reported yield points as approximate values that capture the average stress state required to initiate large-scale irreversible flow in the glass. Finally, we note that some portion of the events we identify as “pre-yield” plastic events could also be reversible elastic

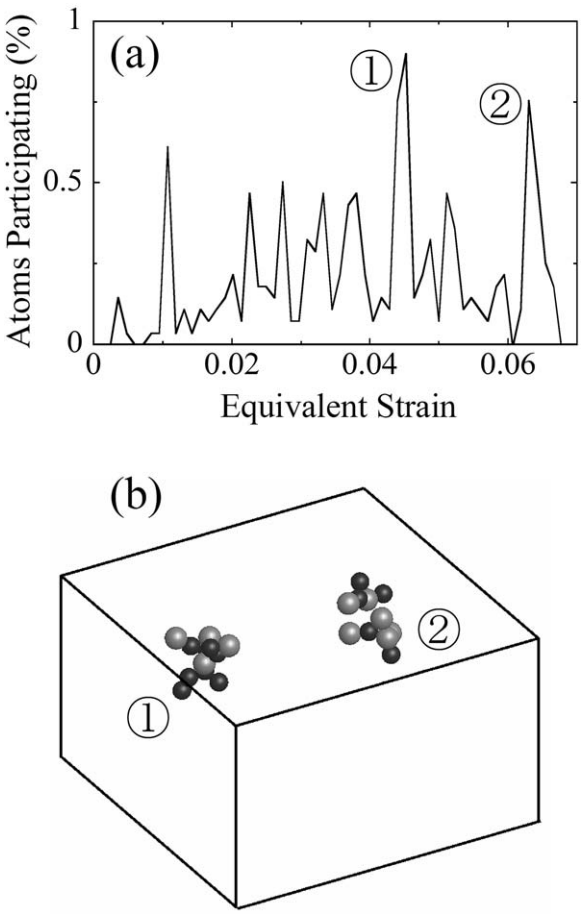

Fig. 5. In (a), the fraction of atoms nominally participating in plastic deformation is shown as a function of the equivalent strain. A visual representation of shear transformation zones (STZs) associated with the two largest peaks in (a) is shown in (b). The labels ① and ② indicate STZ activity at equivalent strains of 0.045 and 0.061, respectively. The frame surrounding the atoms in (b) is 4.5 × 4.5 × 2.6 nm.

events, in the same vein as the reversible anelastic atomic shuffles described in detail by Argon [41]; clearly in the present context, such events could not be time-dependent.

For each large spike of atomic-level activity in Fig. 5a, we have found that the participating atoms are correlated spatially. In Fig. 5b, groups of 10–15 atoms participating in plasticity during two such spikes are shown; the first, at a strain of 0.045, is very close to the identified yield point, while the second, at a strain of 0.060, is in the regime of fully plastic deformation. As expected based on the existing theories [41,42] and previous simulations [25,26,29,30,43] of deformation in metallic glasses, we see that the atoms participating in plastic rearrangement are spatially clustered. These clusters of atoms are the so-called "shear transformation zones" discussed in Section 1, and we can now reasonably conclude that they are carrying the plastic deformation in our simulated metallic glasses. Thus, we have a plastic deformation process fundamentally driven by the operation of STZs, and the behavior of the atoms within STZs can be expected to govern the macroscopic yield behavior of these simulated glasses.

4.2. Macroscopic yield criterion

The most common yield criteria, e.g. the Tresca or von Mises criteria, depend principally on the maximum shear stress τ_{max} experienced by the material, and neglect any effects of hydrostatic pressure, $P = -1/3(\sigma_{xx} + \sigma_{yy} + \sigma_{zz})$, or the stress normal to the plane of shear yielding, σ_n. The Tresca and von Mises criteria are fundamentally similar, but that of Tresca is piecewise linear in the $\sigma_{xx}-\sigma_{yy}$ plane, while the von Mises criterion exhibits curvature. These criteria are particularly appropriate for predicting the onset of plastic deformation in typical polycrystalline metals [44], which is the product of dislocation motion that exhibits only a very small tension–compression asymmetry [45]. For the present purposes, the main feature of interest of these criteria is their symmetry, predicting equal yield stresses in tension or compression, and mirror-symmetry across a line defined by $\sigma_{xx} = -\sigma_{yy}$. Thus, for the discussion to follow, we consider only the piecewise linear Tresca criterion, and do not address the relative merits or demerits of this criterion vis-à-vis the von Mises criterion.

The Tresca criterion is based on the hypothesis that a material will fail when τ_{max},

$$\tau_{max} = \frac{\sigma_{max}-\sigma_{min}}{2} \tag{4}$$

reaches a critical value, the yield stress in pure shear τ. In this case, σ_{max} and σ_{min} are the maximum and minimum values, respectively, of

the principle stresses σ_{xx}, σ_{yy}, and σ_{zz}. As noted above, Eq. (4) describes a yield criterion which is symmetric, predicting yield stresses of the same magnitude in either tension or compression; this prediction is inconsistent with the data in Figs. 3 and 4 for our simulated metallic glass.

In some materials P or σ_n are important influences on plastic deformation, and yield criteria have been developed to account for these factors. These criteria include straightforward modifications of the Tresca or von Mises criteria that include a pressure dependence [38,46], and criteria such as the Mohr–Coulomb that include a dependence on σ_n. All these criteria are similar in that they account for asymmetry of the yield surface such as seen in Fig. 4. Again, as we are interested only in the general importance of non-shear terms in governing the yield behavior, we choose to focus on the fundamental Mohr–Coulomb criterion, which takes the form:

$$\tau_y = \tau - \alpha\sigma_n \tag{5}$$

In this formulation, τ_y is the effective yield stress, τ is the yield stress in pure shear, and α is a system-specific coefficient that quantifies the strength of the normal stress effect. The form of Eq. (5) was originally proposed for yield in granular materials, where an applied normal stress can impede the sliding of particles relative to one another, and hence α represents an effective coefficient of friction. In the limit where $\alpha = 0$, the Mohr–Coulomb criterion (Eq. (5)) devolves into the Tresca criterion, making a comparison between these two models natural.

As described above, shear deformation in metallic glasses is accomplished within STZs by the movement of randomly packed atoms relative to one another. By analogy with the relative motions of particles in a granular solid, the Mohr–Coulomb criterion has been postulated as the governing yield criterion in metallic glasses [7,9,16]. However, with the exception of our preliminary report [47] of the data presented in more detail here, to our knowledge, there has been no theoretical validation of Eq. (5) for metallic glasses. In previous report [47], we considered the deformation of an individual STZ using an elementary structural unit composed of nine atoms interacting via the potentials reported here in Table 1. Through that analysis, which we will not repeat here, we found that the yield behavior of an individual STZ agrees very well with Eq. (5) with an effective coefficient of friction $\alpha \approx 0.12$.

The value of α is directly related to the compression/tension strength differential as [7],

$$\frac{\sigma_C^y}{\sigma_T^y} = \frac{(1+\alpha)^2 + \alpha}{(1+\alpha)^2 - \alpha} \tag{6}$$

Using $\alpha = 0.12$ in Eq. (6) predicts a compression/tension asymmetry of 22%, which is very close to the value of 24% given earlier based on multiple uniaxial tension and compression simulations. Similarly, the value of α governs the shape of the yield surface, which we have plotted in Fig. 6 along with the simulation results. Here, the values of σ_{yy}^y and σ_{xx}^y have been normalized to σ_T^y, and the Tresca and Mohr–Coulomb criteria have been fitted to the data in Figs. 6a and 6b, respectively. The Tresca yield criterion is a poor fit to the data (Fig. 6a), owing to their pronounced compression/tension asymmetry. The Mohr–Coulomb criterion with $\alpha = 0.12$ is a much better fit to the data (Fig. 6b), and captures the compression/tension asymmetry quite well.

To summarize this section, all the above results are consistent with a Mohr–Coulomb criterion for metallic glasses, and suggest that this criterion is intrinsic to the atomic-scale processes involved in glass plasticity. Before proceeding, we note that any yield criterion which incorporates a pressure or normal stress effect could give results inherently similar to the Mohr–Coulomb criterion, and hence could quite likely fit the data in Fig. 4 with reasonable accuracy. Based on our earlier analysis of STZ plasticity [47], we believe that the physical origin of this effect in metallic glasses lies in the principle of "atomistic friction", as embodied in the Mohr–Coulomb criterion.

4.3. Comparison to experiment

It is experimentally difficult to probe plane-stress space uniformly, outside of a few simple geometries which result in known stress states. This difficulty is particularly acute for states of biaxial compression, where the unusual shape of

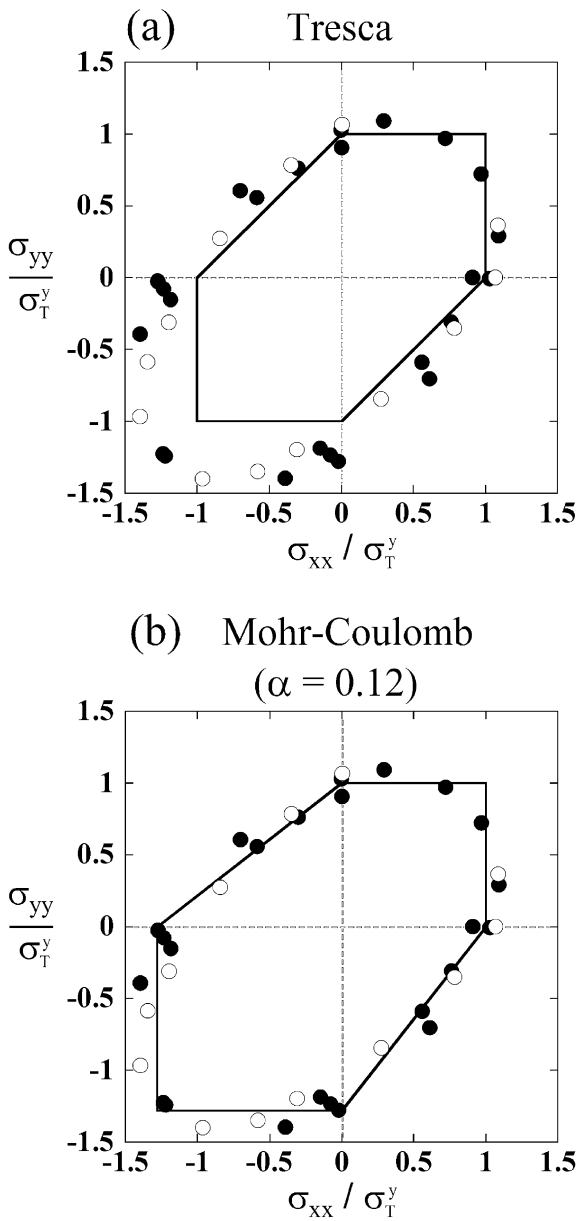

Fig. 6. The 0.5% offset plane-stress yield surface from Fig. 4b fitted to the (a) Tresca and (b) Mohr–Coulomb yield criteria. The Tresca criterion does not account for the observed compression/tension strength asymmetry, while the Mohr–Coulomb criterion does. Solid points and open points represent the data from the 2609 and 2781 atom systems, respectively.

the yield surface is most pronounced in our simulations. As a result, there is a relative scarcity of experimental data for direct comparison to our simulations, and most of the multiaxial yield data which do exist for metallic glasses involve triaxial stress states. Therefore, to facilitate a comparison with experiments, we first replot the data from Fig. 4 in the common manner where the equivalent stress σ_{eq} is given as a function of the stress triaxiality χ at yield. The equivalent stress is defined,

$$\sigma_{eq} \equiv \frac{1}{\sqrt{2}}\sqrt{(\sigma_{xx}-\sigma_{yy})^2 + (\sigma_{xx}-\sigma_{zz})^2 + (\sigma_{yy}-\sigma_{zz})^2} \tag{7}$$

and the stress triaxiality,

$$\chi \equiv \frac{P}{\sigma_{eq}} - \tag{8}$$

In Fig. 7, the data from the present simulations are plotted in this manner, along with the predictions of the Tresca and Mohr–Coulomb criteria in the same form. Again, the Mohr–Coulomb criterion is a reasonable fit, and accounts for the

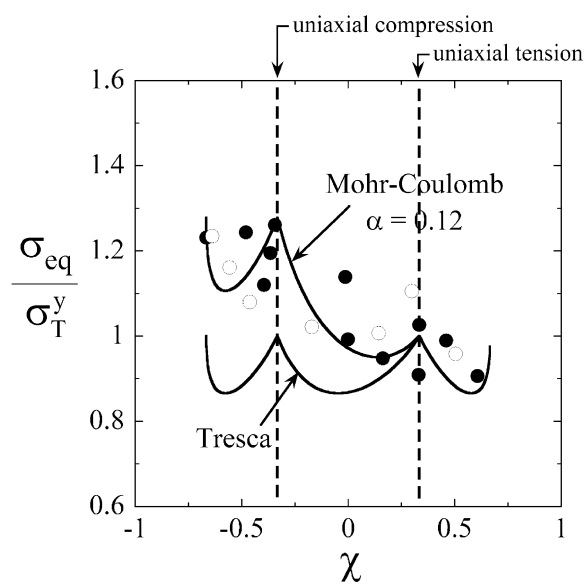

Fig. 7. A plot of the equivalent stress σ_{eq} vs. stress triaxiality χ at yield. Data points (same symbols as in Fig. 6) are from the present simulations, while the lines are the predictions of the Tresca and Mohr–Coulomb criteria (as labeled).

compression/tension asymmetry that the Tresca does not. However, while the simulation data follow the general trend predicted by the Mohr–Coulomb curve, they do not capture the subtleties of the curvature. This apparent departure from the details of the Mohr–Coulomb curve is a different manifestation of the same scatter seen in Fig. 6b, simply made to seem more acute due to the severity of the curvature which results from plotting the data in this manner.

With our simulation data recast in terms of the stress triaxiality, we can now compare our data to the available multiaxial experimental data, as shown in Fig. 8. Donovan [7] studied a $Pd_{40}Ni_{40}P_{20}$ glass in tension, compression, and pure shear. This study identified a compression/tension strength differential of 23%, which compares favorably to the 24% we find in our simulations. Donovan also identified a value of $\alpha = 0.11 \pm 0.03$ from her experiments, in agreement with our value of $\alpha = 0.12$. The data of Lewandowski and coworkers [9] for Zr-based glasses cover a wider variety of stress triaxialities (Fig. 8), owing to their use of combined uniaxial-plus-pressure loading. Their data also show a general trend of higher strength in compression than in tension, albeit far less pronounced than in the data of Donovan [7] or the present simulations. The data of Flores and Dauskardt [13] are not shown in Fig. 8 because the lowest triaxiality they explored was $\chi \approx 0.6$. One final multiaxial experiment not shown in Fig. 8 is the indentation study of Vaidyanathan et al. [16], who matched experimental data with finite element simulations to identify Mohr–Coulomb behavior with $\alpha = 0.13$ for a Zr-based bulk metallic glass. Clearly, although the experimental data exploring multiaxial stress space are limited, they are in general agreement with our simulations.

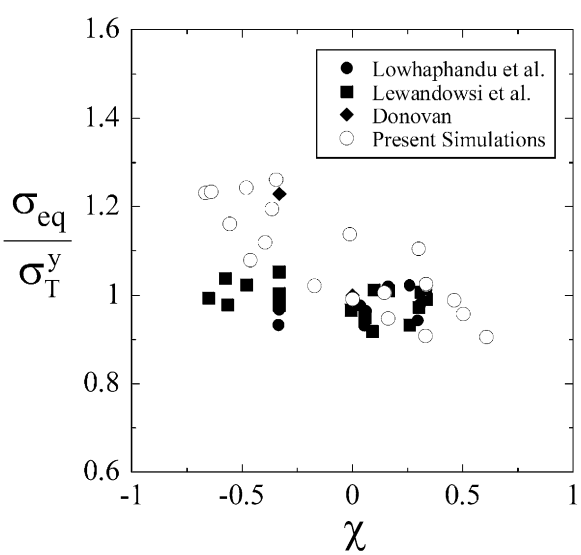

Fig. 8. The equivalent stress vs. stress triaxiality at yield from several experiments and for the present simulation. Original data are from Lowhaphandu et al. [14], Lewandowski et al. [9], and Donovan [7].

We can make additional contact with the experimental literature through the measured angles of shear in tension and compression, θ_T and θ_C respectively, which are directly related to the coefficient α by [16,48],

$$\alpha = \frac{\cos 2\theta_C}{\sin 2\theta_C} = -\frac{\cos 2\theta_T}{\sin 2\theta_T} \tag{9}$$

In Table 2, we list the shear angles of a variety of metallic glasses in tension and/or compression, along with the associated value of α calculated from Eq. (9). The values of α obtained in this manner range from 0 to 0.20 for the compressive shear angles and from 0.11 to 0.49 for the tensile angles.[1] It is not a particular concern that that there is a large range of reported values of fracture angle (and by extension α), as α is expected to be a material specific constant. The value of $\alpha \approx 0.12$ derived from our simulations falls comfortably within the range of calculated values for compressive shear angles, and at the low end of the range for tensile shear in Table 2. What is noteworthy is that the values of α calculated from the compressive shear angles are generally smaller than those calculated from the tensile shear angles; average values for the two cases are $\alpha_C \approx 0.11$ and $\alpha_T \approx$

[1] A compilation of shear angles similar to Table 2 has recently been assembled by Zhang et al. [48], but the reader may notice several discrepancies between these tabulations. In our table, we have been careful to include only unambiguously reported angle measurements from specimens loaded in simple stress states. Furthermore, the data in Table 2 are from monolithic amorphous alloys; some of the data collected by Zhang et al. incorporate nanocrystalline or quasicrystalline inclusions [49,50].

Table 2
Shear angles with respect to the loading axis for multiple metallic glasses, in both uniaxial tension and compression, with the associated value of α calculated from Eq. (9)

Investigator	Material	Tension		Compression	
		θ_T	α	θ_C	α
Zhang et al. [48]	$Zr_{59}Ni_8Cu_{20}Al_{10}Ti_3$	54°	0.32	43°	0.07
Liu et al. [2]	$Zr_{55}Ni_5Cu_{30}Al_{10}$	53–58°	0.29–0.49		
	$Zr_{52.5}Ni_{14.6}Cu_{17.9}Al_{10}Ti_5$	54°	0.32	44–46°	0.03–0
Wright et al. [40]	$Zr_{40}Ni_{10}Cu_{12}Ti_{14}Be_{24}$			42°	0.11
Lewandowski and Lowhaphandu [9]	$Zr_{63.2}Ni_{9.4}Cu_{13.4}Ti_{9.9}Be_{4.1}$	50–53°	0.18–0.29	39.4–41.4°	0.13–0.20
Donovan [7]	$Pd_{40}Ni_{40}P_{20}$			40.7–43.1°	0.15–0.07
Donovan[a] [7]	$Pd_{40}Ni_{40}P_{20}$	50°	0.18	40°	0.18
Mukai et al. [1]	$Pd_{40}Ni_{40}P_{20}$	56°	0.40	42°	0.11
Megusar et al. [10]	$Pd_{80}Si_{20}$	48–50°	0.11–0.18		
Takayama [11]	$Pd_{77.5}Cu_6Si_{16.5}$	51°	0.21		

[a] These angles are for shear banding on the compressive and tensile sides of a 4-point bend specimen.

0.26, respectively. In some cases, these values are significantly different even for the same material and researcher. To some extent, this discrepancy may be related to experimental errors; it is very difficult to accurately measure the fracture angle and the value of α is relatively sensitive to changes of even a few degrees. In particular, accurate measurement of the shear angle requires an observation exactly perpendicular to the shear plane, as well as a correction for the elastic elongation of the specimen at the time of shear. These effects can cause both over- or underestimation, depending on the nature of the loading and the method used to determine the angle. In spite of these potential experimental pitfalls, the systematic nature of the discrepancy observed in Table 2 suggests that something more fundamental is likely at work; this is discussed in more detail below.

In contrast to the experimental data collected in Table 2, our simulation data are well-fitted with just a single value of α in either tension or compression. However, these simulations are highly idealized and neglect many features of true experimental conditions. In an earlier section, we demonstrated that the governing mechanism of plasticity in our simulated glasses is the operation of STZs, and it is important to note that this process occurs *in isolation* in these simulations. The use of small simulation volumes and periodic boundary conditions suppresses many larger-scale features of yielding in metallic glasses, and this provides some clear points of contrast with experiment:

- In macroscopic specimens of bulk metallic glass, the operation of individual STZs is principally relevant in that the STZs self-assemble into macroscopic shear bands [51]. The actual displacement observed in shear bands is usually of the order of several microns [2,40], while an individual STZ operation creates a displacement on the nanometer-scale. Therefore, in experiments, many STZs must operate multiple times within a single shear band to achieve micron-scale displacements.
- Since shear banding requires dilatation of the atomic structure, there is a significant free volume evolution due to plastic deformation. Several recent studies have discussed how these free volume effects should be different under tensile and compressive states of loading [13,52], and detailed transmission electron microscopy studies have observed coalescence of free volume into nanovoids within shear bands [53]. Different fracture surfaces are also observed in tension and compression [48], suggesting that micron or larger-scale processes are affected by the stress state, beyond the simple Mohr–Coulomb dependence of the STZ.

The simulation cells used in this work are simply

too small to capture these larger-scale effects. There are also several differences between simulation and experiments that arise due to our use of completely *athermal* static calculations:

- Many authors have discussed the possibility of adiabatic temperature rise during shear band propagation, and possibly even local melting during fracture events [2,54–56]; our simulations are forced to a temperature of 0 K.
- Several studies have suggested that ordering or recrystallization occurs within shear bands [57,58]; without thermally activated diffusion, these kinds of structural evolutions may not be possible. The same shortcoming could also preclude the coalescence of free volume into voids.

Finally, we note that our idealized simulations are devoid of other possible structural artifacts in actual metallic glasses, including gradients in chemical composition or ordering.

Clearly, all the above effects involve length scales and temperatures that are explicitly precluded in our simulations. While our simulations show that metallic glasses have at least one contribution to yield surface asymmetry in the very fundamental process of STZ operation, we have not excluded the possibility of additional asymmetries that arise from the above processes. We speculate that one or more of these effects may exert an additional pressure or normal-stress dependence on the macroscopic yield of bulk metallic glasses, which may also explain the modest mismatch in the tensile and compressive values of α collected in Table 2.

5. Conclusions

We have performed molecular statics simulations of a model Cu–Zr metallic glass to investigate the elastic–plastic transition under multiaxial loading conditions. The simulated specimens display an initial linear-elastic response, followed by a gradual transition to fully plastic behavior, and they are uniformly stronger in net compressive stress states than they are in net tension. This asymmetry in the plane-stress yield surface can be well-described using the Mohr–Coulomb yield criterion with an effective friction coefficient $\alpha = 0.12$. This value can be linked to the fundamental criterion for operation of a STZ, and analysis of the atomic movements confirms that STZs carry the plastic deformation in our simulated glasses. A comparison between the current simulations and limited multiaxial experiments on metallic glasses reveals reasonable agreement, as does a comparison to the literature based on shear angles.

Acknowledgements

This work was partially supported by the Defense University Research Initiative on Nano-Technology (DURINT) on damage and failure resistant nanostructured materials, which is funded at MIT by the Office of Naval Research, Grant No. N00014-01-1-0808.

References

[1] Mukai T, Nieh TG, Kawamura Y, Inoue A, Higashi K. Intermetallics 2002;10:1071.
[2] Liu CT, Heatherly L, Easton CA, Carmichael CA, Schneibel JH, Chen CH et al. Metall Mater Trans 1998;29A:1811.
[3] Pampillo CA. J Mater Sci 1975;10:1194.
[4] Kimura H, Masumoto T. Acta Metall 1983;31:231.
[5] Donovan PE. Mater Sci Eng 1988;98:487.
[6] Schuh CA, Nieh TG. Acta Mater 2003;51:87.
[7] Donovan PE. Acta Metall 1989;37:445.
[8] He G, Lu J, Bian Z, Chen D, Chen G, Tu G et al. Mater Trans JIM 2001;42:356.
[9] Lewandowski JJ, Lowhaphandu P. Phil Mag 2002;82A:3427.
[10] Megusar J, Argon AS, Grant NJ. Mater Sci Eng 1979;38:63.
[11] Takayama S. Scripta Metall 1979;13:463.
[12] Davis LA, Kavesh S. J Mater Sci 1975;10:453.
[13] Flores KM, Dauskardt RH. Acta Mater 2001;49:2527.
[14] Lowhaphandu P, Montgomery SL, Lewandowski JJ. Scripta Mater 1999;41:19.
[15] Lowhaphandu P, Ludrosky LA, Montgomery SL, Lewandowski JJ. Intermetallics 2000;8:487.
[16] Vaidyanathan R, Dao M, Ravichandran G, Suresh S. Acta Mater 2001;49:3781.
[17] Ertürk T, Argon AS. J Mater Sci 1987;22:1365.
[18] Lund AC, Schuh CA. Appl Phys Lett 2003;82/2017.
[19] Lam NQ, Okamoto PR, Li M. J Nucl Mater 1997;251:89.

[20] Massobrio C, Pontikis V, Martin G. Phys Rev B 1990;41:10486.
[21] Hsieh H, Yip S. Phys Rev Lett 1987;59:2760.
[22] Deng D, Argon AS, Yip S. Phil Trans R Soc Lond 1989;329:549.
[23] Deng D, Argon AS, Yip S. Phil Trans R Soc Lond 1989;329:575.
[24] Perera DN, Harrowell P. Phys Rev 1999;E59:5721.
[25] Deng D, Argon AS, Yip S. Phil Trans R Soc Lond 1989;329:613.
[26] Falk ML. Phys Rev B 1999;60:7062.
[27] Malandro DL, Lacks DJ. J Chem Phys 1999;110:4593.
[28] Gagnon G, Patton J, Lacks DJ. Phys Rev E 2001;64:051508.
[29] Falk ML, Langer JS. Phys Rev 1998;E57:7192.
[30] Srolovitz D, Vitek V, Egami T. Acta Metall 1983;31:335.
[31] Lacks DJ. Phys Rev Lett 2001;87:225502.
[32] Press WH, Teuklosky SA, Vetterling WT, Flannery BP. Numerical recipes in C., 2nd ed. Cambridge: Cambridge University Press, 1992.
[33] Kobayashi S, Maeda K, Takeuchi S. J Phys Soc Japan 1980;48:1147.
[34] Kobayashi S, Maeda K, Takeuchi S. Acta Metall 1980;28:1641.
[35] Born M, Huang K. Dynamical theory of crystal lattices. Oxford, UK: Claredon Press, 1954.
[36] Raghava R, Cadell RM, Yeh GSY. J Mater Sci 1973;8:225.
[37] Li JCM. Treat Mater Sci 1981;20:325.
[38] Rottler J, Robbins MO. Phys Rev 2001;E64:051801.
[39] Inoue A. Acta Mater 2000;48:279.
[40] Wright WJ, Saha R, Nix WD. Mater Trans JIM 2001;42:642.
[41] Argon AS. Acta Metall 1979;27:47.
[42] Spaepen F. Acta Metall 1977;25:407.
[43] Argon AS, Kuo HY. Mater Sci Eng 1979;39:101.
[44] Courtney TH. Mechanical behavior of materials. New York: McGraw-Hill, 1990.
[45] Bulatov VV, Richmond O, Glazov MV. Acta Mater 1999;47:3507.
[46] Argon AS. Inelastic deformation and fracture of glassy solids. In: Cahn RW, Haasen P, Kramer EJ, editors. Materials science and technology. Weinheim, Germany: VCH; 1993. p. 46-1.
[47] Schuh CA, Lund AC. Nat Mater 2003;2:449.
[48] Zhang ZF, Eckert J, Schultz L. Acta Mater 2003;51:1167.
[49] Fan C, Inoue A. Mater Trans JIM 1999;40:1376.
[50] Inoue A, Kimura HM, Zhang T. Mater Sci Eng 2000;294–296:727.
[51] Bulatov VV, Argon AS. Modell Simul Mater Sci Eng 1994;2:203.
[52] Wright WJ, Hufnagel TC, Nix WD. J Appl Phys 2003;93:1432.
[53] Li J, Spaepen F, Hufnagel TC. Phil Mag 2002;A82:2623.
[54] Wright WJ, Schwarz RB, Nix WD. Mater Sci Eng 2001;A319–321:229.
[55] Flores KM, Dauskardt RH. J Mater Res 1999;14:638.
[56] Flores KM, Dauskardt RH. Mater Sci Eng 2001;A319–321:511.
[57] Chen H, He Y, Shiflet GJ, Poon SJ. Nature 1994;367:541.
[58] Kim J-J, Choi Y, Suresh S, Argon AS. Science 2002;295:654.